

2000 Mathematics Subject Classification: 76V05 (35R35, 65M06)

Keywords: Free boundary model, parabolic problems, finite difference methods, corrosion, copper, brochantite, cultural heritage

A MATHEMATICAL MODEL OF COPPER CORROSION

F. CLARELLI, B. DE FILIPPO, AND R. NATALINI

ABSTRACT. A new partial differential model for monitoring and detecting copper corrosion products (mainly brochantite and cuprite) is proposed to provide predictive tools suitable for describing the evolution of damage induced on bronze specimens by sulfur dioxide (SO_2) pollution. This model is characterized by the movement of a double free boundary. Numerical simulations show a nice agreement with experimental result.

1. INTRODUCTION

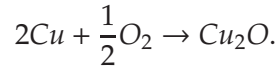
Deterioration of copper and bronze artifacts is one of the main concerns for people working in cultural heritage [25]. More specifically, bronze, a copper-tin alloy, has been widely employed for daily-use and artistic purposes from the Bronze Age up to present. Conservation studies are based on a knowledge of the environmental conditions to which copper and copper alloys may be exposed and include all the information on the material technologies and the nature of the corrosion films or patina, which cover their surfaces. In particular a significant effort has been devoted to study the corrosion due to environmental conditions, such as temperature, moisture, concentration of pollutants [3, 19, 11]. Although in recent years air pollution in European urban areas has decreased considerably, there still remain concentrations of pollutants such as sulfur dioxide (SO_2) from combustion of fossil fuels, being one of the most important factors in the deterioration of bronze. Indeed SO_2 , mixed with water vapor, reacts to produce sulfate acid (H_2SO_4), which causes corrosion phenomena on copper surfaces and produces several corrosion products as basic copper sulphates, such as antlerite, posnjakite, brochantite [14]. The latter is the final product of several reaction steps, which can be approximated by two main chemical reactions: cuprite formation, which occurs after a few weeks of exposure to atmospheric conditions, and brochantite formation, which the final reaction step (for more details on chemical background see Section 2.1) [10].

The complexity of corrosion processes creates the necessity for a quantitative model approach to develop predictive tools, which simultaneously provide both quantitative information as well as simulations of the various processes involved. These methods, similar to those introduced in [6], are useful for the monitoring and detection of surface alterations even before they are visible, making it possible to determine optimal intervention strategies. In this paper we introduce a new partial differential model, which is used to describe the evolution of damage induced on a bronze specimen by atmospheric pollution. It is based on fluid dynamical and chemical relations and it is characterized by a

double free boundary: one between copper and cuprite, the other between cuprite and brochantite. Its calibration has been elaborated according to the experimental results in [7]. The paper is organized as follows: in the Section 2.1 we analyze the main chemical corrosion phenomena and in Section 2.2 we review the main mathematical models already proposed in literature. ...The section 3 is entirely focused on the description of the model's equations and the numerical schemes used, meanwhile in section 4 we describe the experimental setting and the calibration of the model. Finally, in section 5, we present the main results related to the simulations produced by our model and in section 6 the related conclusions.

2. MODELING BACKGROUNDS

2.1. Chemical backgrounds. Most of the oxidation processes occurring on bronze metal artifacts, when exposed to environmental conditions, are electrochemical and involve interactions between the metal surface, the adsorbed moisture and various atmospheric gases (SO_2 , CO_2 , NO_x , hydrocarbons) [22]. Electrochemical corrosion processes in electrolyte and condensed moisture layers have been the subject of extensive studies, based on numerous and different approaches [28, 24, 5]. When exposed to the atmosphere, copper and its alloys form a thin layer of corrosion, from brownish-green up to greenish-blue colors, which is designated as patina. In the case of copper in a low pollutant levels atmosphere, a native cuprite (copper(I) oxide or Cu_2O) film of approximately a few nanometers thick, protects the metal surface from further oxidation. The general reaction is well described in literature, where, in aerated solution, copper can dissolve electrochemically forming copper(I) oxide formation, due to the reaction of copper with oxygen. It is represented by the following schematic reaction [18]:



However, in an aggressive environment, like urban atmosphere, the protective nature of this oxide layer is altered and there is the formation of a non-protective, multi-component, tarnish layer. When the copper is exposed to humidity and sulfur dioxide, three kinds of basic copper sulfate hydroxide are mainly produced: Brochantite $Cu_4SO_4(OH)_6$, which is a well-known patina constituent, or other similar products like Antlerite or Posnjakite. In the following we focus our attention to the formation of Brochantite, which is the main observed product. Gaseous sulfur dioxide and sulfate particles are deposited on the electrolyte on the cuprite. Their deposition reduces the pH of the adsorbed water, and this promotes the dissolution of cuprous ion (Cu^+) and its oxidation, thus forming cupric ions (Cu^{2+}). In detail, copper(I) ions in solution disproportionate to give copper(II) ions and a precipitate of copper (1):



When the cupric and sulfate ion concentrations in the electrolyte are high enough to form brochantite, this phase starts to precipitate on the cuprite [1, 16]. In [20] it is indicated that, in the initial oxidation process, cuprite

formation is followed by posnjakite, as a precursor phase to brochantite, see also [27], but we are going to neglect this intermediate transformations, due to the elevated speed of the reaction with respect to the time scale of the mathematical model which we are going to present.

2.2. Existing mathematical models. Graedel and his collaborators [15, 26] have studied atmospheric copper sulfidation at *AT&T* Bell Laboratories in both experimental investigation and physical or mechanistic model development; furthermore a systematic investigation of copper sulfidation kinetics has been performed. In the paper [26] Tidblad and Graedel developed a model able to describe the SO_2 copper corrosion. Their work is based on aqueous chemistry and without considering spatial dimensions. In the paper [21], they introduce a model which describes the corrosion of copper exposed to moist air with a low SO_2 concentration. Here, they consider four stages in the development of a corrosion patina: the metal, a non-protective oxide film which has a high ionic transport property, an outer layer of corrosion products which can permit the penetration of water and gases and an external adsorbed water layer. More recently, Larson proposed in [17] a different model that describes the atmospheric sulfidation of copper by proposing a physical copper-sulfidation model that includes four distinct phases: the substrate metal, a cohesive cuprous sulfide (Cu_2S) product layer, a thin aqueous film adsorbed on the sulphide and the ambient gas. Larson postulated that transport through the sulfide layer occurs via diffusion and electromigration of copper vacancies and electron holes. Later, in the 1990s, copper sulfation by SO_2 was investigated by Payer et al., who focused their attention on the early stage of corrosion in moist air (75% RH at 25°C) with a sulfur dioxide concentration of 0.5%. The techniques employed (SEM, AES and TEM) allowed for an analysis and characterization of the oxide film (composed of cuprous oxide, copper sulfate and sulfide) on copper surfaces and for the mechanism of evolution of the corrosion chemistry to be described [3]. In the last decade the effect of sulfur dioxide in acid rain on copper and bronze has been investigated. Robbiola and his co-workers studied the effect of its cyclic action on bronze alloys, underlining the different types of patina formed in "sheltered" and "unsheltered" areas of bronze monuments [4, 5].

Subsequently, Larson refined the copper-sulfidation model by focusing on the transport of charged lattice defects in a growing Cu_2S product layer between the ambient gas and the substrate metal. As previously, this transport is postulated to occur via both diffusion and electromigration.

3. THE MODEL

In this section, we aim to introduce a mathematical model able to describe the corrosion effects on a copper layer, which is subject to deposition of SO_2 . The present model is based on the mathematical approach used in [6]. We assume to have a copper sample on which is formed a non protective oxide layer (Cu_2O), and, over this layer, a corrosion product (brochantite) grows. Over the brochantite layer is assumed to be the atmospheric air with SO_2 . An example of these three layers can be seen in Figure 1.

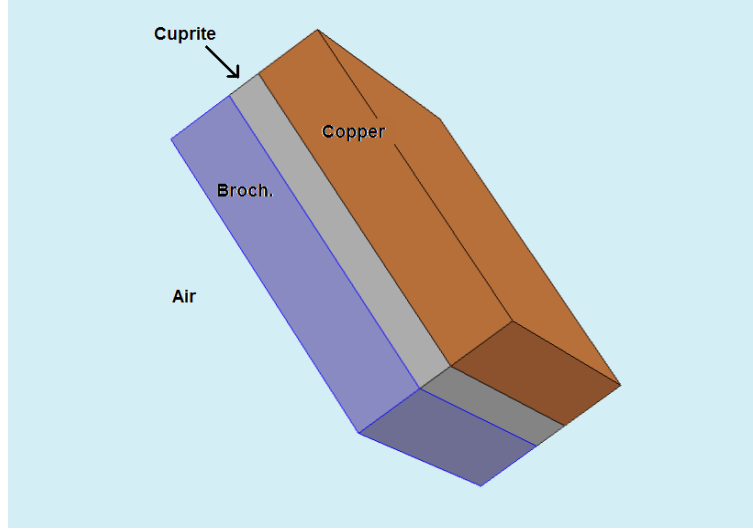


FIGURE 1. Example of cuprite and brochantite deposition on a copper sample.

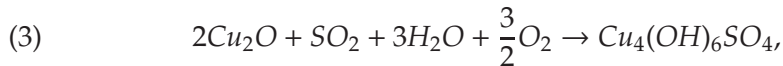
The reaction producing cuprite Cu_2O , can be approximated by



Namely, two moles of copper combined with one-half mole of oxygen produce cuprite.

Laboratory tests, with high concentration of SO_2 and high relative humidity, near to 100%, show that brochantite is the primary product of the reaction, thus it can be considered as the final state reached by the whole reaction.

The overall simplified reaction of brochantite formation can be approximate by the following reaction (3)



where two moles of cuprite combined with three moles of water and three-halves of oxygen produce one mole of brochantite.

In the following, we assume that these two reactions are instantaneous; thus, we obtain a sharp free boundary between cuprite and the unreacted copper, due to the reaction (2), and a second free boundary between brochantite and cuprite, due to the reaction (3).

Assuming these two reactions as instantaneous, the effective time of reaction is implicitly included in the diffusivity coefficients.

3.1. Swelling. We indicate the copper consumption by $a(t)$. The production of Cu_2O on the boundary between copper and the oxide layer proceeds since the water and the oxygen diffuse through the oxide layer. On the upper boundary of cuprous oxide, a brochantite layer begins to form. It is assumed that, in the climatic chamber at a 100% of RH, a thin film of water (with SO_2 dissolved) is formed over the cuprous oxide, and it plays an important role in both reactions. By these assumptions, the consumption of Cu_2O and the

production of brochantite on the upper boundary between oxide and water film occurs. The volume of cuprite consumption is $b(t)$.

The transformation of copper into Cu_2O , such as the transformation of cuprite in brochantite, are accompanied by a volume change (swelling rate). The swelling rate can be calculated easily, because the molar ratio in reaction (1) between Cu and Cu_2O is 2 : 1. Thus two moles of copper change into one mole of Cu_2O , and a different volume of the new matter formed is obtained. The swelling of reaction (1) is

$$(4) \quad \dot{a}_e = -\omega_p \dot{a};$$

where a_e is the swelling of reaction (1), and

$$(5) \quad \omega_p = \frac{\mu_c}{2\mu_p} - 1$$

represents the expansion volume ratio; μ_c and μ_p being the molar density (*moles/cm³*) of Cu and Cu_2O respectively. It is assumed that μ_c and that μ_p are constant (i.e. they are homogeneous materials). Under these assumptions, if $a_e(0) = a(0) = 0$, then it is possible to conclude that

$$(6) \quad a_e(t) = -\omega_p a(t),$$

and the thickness of cuprite layer $h_p(t)$, is proportional to the copper consumption $a(t)$

$$(7) \quad h_p(t) = (1 + \omega_p) a(t).$$

On the external boundary of cuprite, we assume that SO_2 reacts with Cu_2O in presence of water, see reaction (3). Here, we have that 2 moles of cuprite change in 1 mole of brochantite, wasting 1 mole of SO_2 , 3 moles of H_2O and 3/2 moles of oxygen. Thus, the brochantite layer grows on the external boundary of cuprite, and we indicate the external boundary of brochantite with $\gamma(t)$.

As in equation (6), the swelling rate of brochantite is given by

$$(8) \quad \dot{b}_e(t) = -\omega_b \dot{b}(t);$$

where $b_e(t)$ is the swelling of reaction (3),

$$(9) \quad \omega_b = \frac{\mu_p}{2\mu_b} - 1,$$

and μ_b is the constant molar density of brochantite.

The cuprite consumption $b(t)$ is referred to a system of reference at rest, but we have to take into account the moving cuprite boundary. The physical boundary between cuprite and brochantite is given by

$$(10) \quad \beta(t) = b(t) + a_e(t),$$

where $b(t)$ is the consumption of cuprite (assumed to be positive such as $a(t)$), then $a_e < 0$, see eq. (6). Thus, the variation of the overall external boundary γ is given by

$$(11) \quad \dot{\gamma} = -\omega_p \dot{a}(t) - \omega_b \dot{b}(t).$$

Summarizing, the geometry of our problem is one-dimensional, and we have 4 regions (e.g. see figure 2):

- (1) Copper (inner region).
- (2) Cuprite Cu_2O , between $a(t)$ and $\beta(t)$.
- (3) Brochantite $Cu_4(OH)_6SO_4$, between $\beta(t)$ and $\gamma(t)$.
- (4) Water film and air on the external side of $\gamma(t)$.

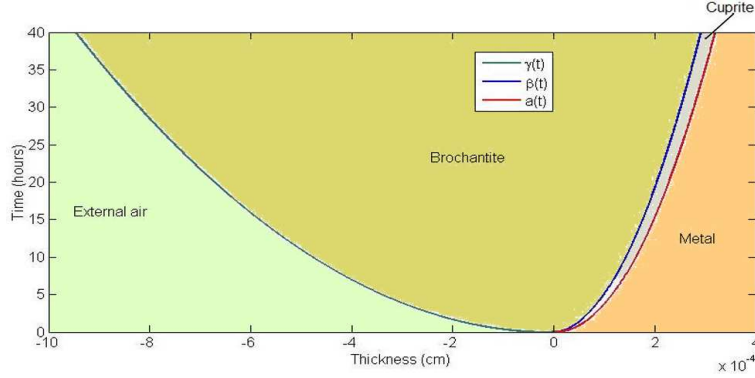


FIGURE 2. Example of cuprite and brochantite theoretical growth (in time) on a copper sample.

3.2. Equation of the model. It is well known that relative humidity plays a key role in regulating the speed of oxydation and sulfation. It has been observed that when relative humidity exceeds some threshold, then SO_2 reacts completely such as the oxidation of copper happens with full speed. We can interpret this phenomenon as follows. According to eq. (3), when a molecule of SO_2 comes in contact with cuprite, it reacts if three molecules of H_2O are available at the same point (we suppose that there is always enough O_2). To be more precise, this is true only if vapor condenses on the unreacted specimen surface forming a liquid film, and this happens with high relative humidity values.

The brochantite formation (eq. (3)) has been assumed to develop on the cuprite layer, due to the SO_2 , H_2O and O_2 , which move through the brochantite layer and react with Cu_2O . This reaction implies a wasting of Cu_2O , with the formation of a new layer of brochantite. Summarizing, the region of brochantite is given by $\gamma(t) \leq x \leq \beta(t)$ and the region of Cu_2O is $\beta(t) \leq x \leq a$.

Let's denote the concentration of SO_2 in the pores of brochantite by S , coming from the external air, such as the water concentration indicated by W and the oxygen concentration by O throughout brochantite and by G throughout cuprite.

The flow of SO_2 relative to air is governed by Fick's law. Thus, in the frame of reference where copper is at rest, the SO_2 flux has the following expression

$$(12) \quad J_s = n_b \left(-D_s \frac{\partial S}{\partial x} - S\omega_p \dot{a} - S\omega_b \dot{b} \right) = n_b \left(-D_s \frac{\partial S}{\partial x} + S\dot{\gamma} \right),$$

where the first term refers to SO_2 diffusion in the brochantite layer, D_s is the diffusivity, the second and the third terms on the left side refer to the swelling caused by cuprite and brochantite formation respectively.

Hence the mass balance of SO_2 in the brochantite layer $\gamma(t) \leq x \leq \beta(t)$ is

$$(13) \quad \frac{\partial S}{\partial t} - D_s \frac{\partial^2 S}{\partial x^2} + \dot{\gamma} \frac{\partial S}{\partial x} = 0;$$

The value of S at the external boundary $\gamma(t)$ is the environment SO_2 concentration $S_a(t)$, which is a known function of time

$$(14) \quad S(\gamma(t)) = S_a(t);$$

We assumed that SO_2 reacts totally with Cu_2O at the front $\beta(t)$, thus we have

$$(15) \quad S(\beta(t)) = 0.$$

Now, we need of further condition (first free boundary). Since the SO_2 flux of moles at the boundary $\beta(t)$ is proportional to Cu_2O moles consumption, we have

$$(16) \quad -n_b \frac{D_s}{M_s} \frac{\partial S}{\partial x} = \frac{1}{2} \frac{\rho_p}{M_p} \dot{b};$$

where M_s, M_p are the molar weight of SO_2 and Cu_2O respectively, ρ_p is the mass density of cuprite.

Similarly, the water flux is

$$(17) \quad J_w = n_b \left(-D_w \frac{\partial W}{\partial x} - W \omega_p \dot{a} - W \omega_b \dot{b} \right) = n_b \left(-D_w \frac{\partial W}{\partial x} + W \dot{\gamma} \right),$$

where D_w is the water diffusivity. Thus, the mass balance in the brochantite layer is

$$(18) \quad \frac{\partial W}{\partial t} - D_w \frac{\partial^2 W}{\partial x^2} + \dot{\gamma} \frac{\partial W}{\partial x} = 0.$$

The value of W at the external boundary $\gamma(t)$ is the environment water concentration $W_a(t)$

$$(19) \quad W(\gamma(t)) = W_a(t);$$

Since some moles of water are wasted by the reaction (3), at the front $\beta(t)$ we have

$$(20) \quad \frac{J_w}{M_w} = \frac{3}{2} \frac{\rho_p}{M_p} \dot{b} + n_b \frac{W}{M_w} \dot{b}.$$

Finally, the oxygen flux is

$$(21) \quad J_o = n_b \left(-D_o \frac{\partial O}{\partial x} + O \dot{\gamma} \right),$$

where D_o is the oxygen diffusivity. Thus, the mass balance in the brochantite layer is

$$(22) \quad \frac{\partial O}{\partial t} - D_o \frac{\partial^2 O}{\partial x^2} + \dot{\gamma} \frac{\partial O}{\partial x} = 0.$$

The value of O at the external boundary $\gamma(t)$ is the environment oxygen concentration $O_a(t)$

$$(23) \quad O(\gamma(t)) = O_a(t).$$

Since the oxygen is also wasted by the reaction (3), at the front $\beta(t)$ we have

$$(24) \quad \frac{J_o}{M_o} = \frac{3}{4} \frac{\rho_p}{M_p} \dot{b} + n_b \frac{O}{M_o} \dot{b}.$$

3.3. Cuprite layer equations. We assumed that the reaction between oxygen and copper occurs on the copper-cuprous oxide boundary $\alpha(t)$. Here, we indicate oxygen by G , just to avoid confusion with the previous region. We make a mass balance of oxygen concentration G , and we assume that all oxygen moles arriving on the inner boundary $a(t)$ react. This assumption is not really true, in fact the water plays a key role in the speed of reaction, but in our experiments we have a relative humidity near to 100%, and this fact justify our assumption; also, the diffusivity D_g includes implicitly the finite time of reaction.

The flux of oxygen is

$$(25) \quad J_g = n_p \left(-D_g \frac{\partial G}{\partial x} - G \omega_p \dot{a} \right),$$

and the mass balance equation is

$$(26) \quad \frac{\partial G}{\partial t} - D_g \frac{\partial^2 G}{\partial x^2} - \omega_p \dot{a} \frac{\partial G}{\partial x} = 0.$$

The value of G at the boundary $\beta(t)$ is given by the value of oxygen on the boundary β , given by eq. (24).

$$(27) \quad G(\beta(t)) = O(\beta(t));$$

Since oxygen reacts totally with copper at the boundary $a(t)$, we have

$$(28) \quad G(a(t)) = 0;$$

Now, we need further condition to close the system (second free boundary). Since the oxygen react totally at the boundary $\alpha(t)$, the copper moles wasted are given by

$$(29) \quad -n_p \frac{D_g}{M_g} \frac{\partial G}{\partial x} = \frac{1}{4} \frac{\rho_c}{M_c} \dot{a}.$$

3.4. Rescaling. The geometry of the problem is given by two regions, one is given by $x \in [\beta(t), a(t)]$ which describes the layer of Cu_2O , the other is given by $x \in [\gamma(t), \beta(t)]$ i.e. the brochantite layer. Also we have $\dot{\gamma} = -(\omega_p \dot{a} + \omega_b \dot{b})$.

3.4.1. New variables. In the first region we adopt $(x, t) \rightarrow (y, \tau)$, in the second one $(x, t) \rightarrow (z, \tau)$. We find out

$$(30a) \quad y = \frac{x - \beta}{a - \beta}; \quad \partial_x = 1/(a - \beta) \partial_y, \quad \partial_{xx} = 1/(a - \beta)^2 \partial_{yy}, \quad \partial_t = f(t) \partial_y + \frac{1}{t_r} \partial_\tau;$$

$$(30b) \quad z = \frac{x - \gamma}{\beta - \gamma}; \quad \partial_x = 1/(\beta - \gamma) \partial_z, \quad \partial_{xx} = 1/(\beta - \gamma)^2 \partial_{zz}, \quad \partial_t = q(t) \partial_z + \frac{1}{t_r} \partial_\tau;$$

where

$$(31a) \quad f(y, \tau) = \frac{1}{t_r} \frac{y(\partial_\tau \beta - \partial_\tau a) - \partial_\tau \beta}{a - \beta},$$

$$(31b) \quad q(z, \tau) = \frac{1}{t_r} \frac{z(\partial_\tau \gamma - \partial_\tau \beta) - \partial_\tau \gamma}{\beta - \gamma}.$$

Now, we rescale the following parameters and variables in non-dimensional form:

$$(32a) \quad \hat{W} = \frac{W}{W_r}, \quad \hat{G} = \frac{G}{G_r}, \quad \hat{S} = \frac{S}{S_r}, \quad \hat{a} = \frac{a}{\lambda}, \quad \hat{b} = \frac{b}{\lambda}, \quad \hat{\beta} = \frac{\beta}{\lambda}, \quad \hat{\gamma} = \frac{\gamma}{\lambda},$$

$$(32b) \quad \hat{D}_g = \frac{t_r}{\lambda^2} D_g, \quad \hat{D}_w = \frac{t_r}{\lambda^2} D_w, \quad \hat{D}_s = \frac{t_r}{\lambda^2} D_s, \quad \hat{q}(z, \tau) = t_r q, \quad \hat{f}(y, \tau) = t_r f$$

From now on, we assume that dotted variables are derivatives with respect to the dimensionless time τ ($\dot{V} = dV/d\tau$).

Assuming $\Omega_s = 2n_b \hat{D}_s \frac{M_p S_r}{M_s \rho_p}$, $\Gamma_w = \frac{3}{2} \frac{1}{n_b} \frac{M_w \rho_p}{M_p W_r}$, $\Omega_g = 4n_p \hat{D}_g \frac{M_c G_r}{M_g \rho_c}$. Also, $\dot{\gamma} = -(\omega_p \hat{a} + \omega_b \hat{b})$, the non-dimensional system is:

3.4.2. *Outer region.* For $\gamma \leq x \leq \beta \rightarrow 0 \leq z \leq 1$

$$(33) \quad \frac{\partial \hat{S}}{\partial \tau} = \frac{\hat{D}_s}{(\hat{\beta} - \hat{\gamma})^2} \frac{\partial^2 \hat{S}}{\partial z^2} - \left(\frac{\dot{\gamma}}{(\hat{\beta} - \hat{\gamma})} + \hat{q} \right) \frac{\partial \hat{S}}{\partial z},$$

$$(34) \quad \hat{S}(0, \tau) = \hat{S}_a.$$

$$(35) \quad \hat{S}(1, \tau) = 0,$$

$$(36) \quad -\frac{\Omega_s}{(\hat{\beta} - \hat{\gamma})} \frac{\partial \hat{S}}{\partial z}(1, \tau) = \dot{b},$$

$$(37) \quad \frac{\partial \hat{W}}{\partial \tau} = \frac{\hat{D}_w}{(\hat{\beta} - \hat{\gamma})^2} \frac{\partial^2 \hat{W}}{\partial z^2} - \left(\frac{\dot{\gamma}}{(\hat{\beta} - \hat{\gamma})} + \hat{q} \right) \frac{\partial \hat{W}}{\partial z},$$

$$(38) \quad \hat{W}(0, \tau) = \hat{W}_a(\tau).$$

$$(39) \quad \frac{\hat{D}_w}{(\hat{\beta} - \hat{\gamma})} \frac{\partial \hat{W}}{\partial z}(1, \tau) = (\dot{\gamma} - \dot{b}) \hat{W} - \frac{3}{2n_b} \frac{\rho_p M_w}{W_r M_p} \dot{b};$$

$$(40) \quad \frac{\partial \hat{O}}{\partial \tau} = \frac{\hat{D}_o}{(\hat{\beta} - \hat{\gamma})^2} \frac{\partial^2 \hat{O}}{\partial z^2} - \left(\frac{\dot{\gamma}}{(\hat{\beta} - \hat{\gamma})} + \hat{q} \right) \frac{\partial \hat{O}}{\partial z},$$

$$(41) \quad \hat{O}(0, \tau) = \hat{O}_a(\tau).$$

$$(42) \quad \frac{\hat{D}_o}{(\hat{\beta} - \hat{\gamma})} \frac{\partial \hat{O}}{\partial z}(1, \tau) = (\hat{\gamma} - \hat{b}) \hat{O} - \frac{3}{4m_b} \frac{\rho_p}{O_r} \frac{M_o}{M_p} \hat{b},$$

3.4.3. *Inner region.* For $\beta \leq x \leq a \rightarrow 0 \leq y \leq 1$,

$$(43) \quad \frac{\partial \hat{G}}{\partial \tau} = \frac{\hat{D}_g}{(\hat{a} - \hat{\beta})^2} \frac{\partial^2 \hat{G}}{\partial y^2} + \left(\omega_p \frac{\hat{a}}{\hat{a} - \hat{\beta}} - \hat{f}(y, \tau) \right) \frac{\partial \hat{G}}{\partial y},$$

(we have to highlight that \dot{a} is a derivative with respect to the τ)

$$(44) \quad \hat{G}(1, \tau) = 0,$$

$$(45) \quad \hat{G}(0, \tau) = \hat{O}|_{\beta},$$

$$(46) \quad -\frac{\Omega_w}{\hat{a} - \hat{\beta}} \frac{\partial \hat{G}}{\partial y} = \dot{\hat{a}}.$$

From now on we use the non-dimensional system, so we indicate all non-dimensional terms without hat.

3.5. Numerical solutions. To solve our model, we have to set up an appropriate numerical scheme which is able to describe the process in a short range of time (about 40 hours), but also simulations of 1 year taking under control the numerical stability. For these reasons we use finite differences schemes with implicit-explicit terms. It can be found in [2] and [23].

3.5.1. *Initial conditions.* Our numerical procedure requires $a(0) \neq 0$ and $\beta(0) \neq a(0)$ to avoid singularities in the internal region confining with copper. By physical assumption, we know that $a(0) > 0$ because it represents the first copper consumption. In order that the external equations work (SO_2 is present), we need to set up $\beta(0) > 0$ and $\gamma(0) \neq \beta(0)$.

3.5.2. *Numerical scheme.* Indicating explicit term as $H(U)$ and implicit term by $G(U)$, we present our system in the external region (eqs. 33-39) in the following form

$$(47) \quad U_t = H(U) + G(U);$$

where

$$U = \begin{pmatrix} S \\ W \\ O \end{pmatrix},$$

the explicit term $H(U)$ is

$$H(U) = \begin{pmatrix} -\left(\frac{\dot{\gamma}}{(\beta - \gamma)} + q\right) \frac{\partial S}{\partial z} \\ -\left(\frac{\dot{\gamma}}{(\beta - \gamma)} + q\right) \frac{\partial W}{\partial z} \\ -\left(\frac{\dot{\gamma}}{(\beta - \gamma)} + q\right) \frac{\partial O}{\partial z} \end{pmatrix},$$

and the implicit term $G(U)$ is

$$G(U) = \begin{pmatrix} \frac{D_s}{(\beta - \gamma)^2} \frac{\partial^2 S}{\partial z^2} \\ \frac{D_w}{(\beta - \gamma)^2} \frac{\partial^2 W}{\partial z^2} \\ \frac{D_o}{(\beta - \gamma)^2} \frac{\partial^2 O}{\partial z^2} \end{pmatrix},$$

since $G(U)$ is a stiff term which will be integrated implicitly to avoid excessively small time steps.

A more general scheme is IMEX-DIRK Runge-Kutta, which is given by, for $t = n\Delta t$,

$$(48) \quad u^{(i)} = u^n + \Delta t \sum_{k=1}^{i-1} \tilde{a}_{ik} H(u^{(k)}) + \Delta t \sum_{k=1}^i a_{ik} G(u^{(k)}), \quad i = 1, \dots, v$$

$$(49) \quad u^{n+1} = u^n + \Delta t \sum_{i=1}^v \tilde{\omega}_i H(u^{(i)}) + \Delta t \sum_{i=1}^v \omega_i G(u^{(i)}).$$

Here, the matrices $\tilde{A} = (\tilde{a}_{ik})$, where $\tilde{a}_{ik} = 0$ for $j \geq i$ and $A = (a_{ik})$ are $v \times v$ matrices such that the resulting scheme is explicit in H and implicit in G. The DIRK formulation requires $a_{ik} = 0$ for $j > i$ [2].

Following the IMEX formalism we shall use the notation $\text{Name}(s; v; p)$ to identify a scheme, where s is the number of stages of the implicit scheme, v is the number of explicit stages and p is the combined order of the scheme. In our case we choose to use an Implicit-Explicit Midpoint(1,2,2): $s = 1$, $v = 2$ and $p = 2$.

By the same method, and at the same time-step of previous integration, we integrated also equations (43)-(46).

4. ASSESSMENT OF THE MODEL

4.1. Experiments. The calibration of the model has been made with reference to a precise experimental campaign, which is described in [7], where the main characteristics of the experimental setting are reported. Experiments were carried out in a cyclic corrosion cabinet (Erchisen Mod. 519/AUTO) and the $\text{Cu} - 12\text{Sn}$ cast bronze specimens were chosen as a representative alloy used in the past (ancient Greek type). For the corrosion test, all bronze specimens were exposed to an atmosphere containing about 200 ppm of SO_2 at 40°C and 100% RH for 8 hours (wet cycle), subsequently they were exposed to room conditions for 16 hours (dry cycle). Each wet and dry cycle was repeated 20 times. The measures of patina thickness, useful for the model calibration, were performed using a SEM-EDS instrument

TABLE 1. Parameters table

Param.	Value	Dimension	Indications
ρ_p	6.00	g/cm^3	Cu_2O mass density
M_p	143.09	g/mol	Cu_2O molar mass
ρ_c	8.94	g/cm^3	Copper mass density
M_c	63.55	g/mol	Copper molar mass
ρ_b	3.97	g/cm^3	Brochantite mass density
M_b	452.3	g/mol	Brochantite molar mass
ρ_s	1.46	g/cm^3	SO_2 mass density
M_s	64.07	g/mol	SO_2 molar mass

equipped with an Image Analyzer (IA). Each measurement (after 8, 24 and 40 hours) has been obtained by an average of 20 measures.

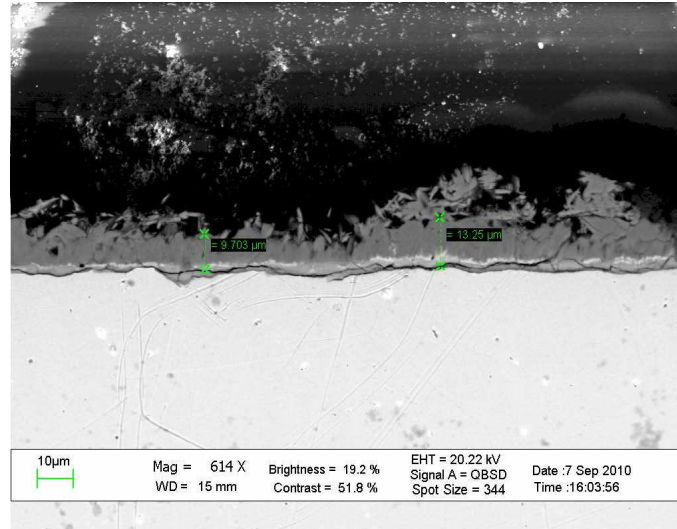


FIGURE 3. Example of patina thickness measurement with the SEM employment. From [7]

The early stage of exposure of bronze samples mainly produced copper hydroxyl-sulfate (brochantite and chalcantite), cuprous oxide, and tin sulfide (ottemannite). The tarnish product layer also contained a trace of tin oxide. As determined by XRD analysis, the brochantite formation was predominant with the increase of the number of corrosion cycles. Otherwise, the chalcantite formation was detected during the early stage of the corrosion processes and the intensity of its characteristic peaks decreases as a function of time. The same consideration can be made for the ottemannite formation, detected with SEM-EDS in localized micro-crack areas, which are rapidly covered by basic copper sulfates [7, 8].

4.2. Calibration. The laboratory corrosion tests has been used to calibrate the model. We suppose that the parameters to calibrate by experimental tests are the diffusivity coefficients. To do that, we used the thickness of

corrosion products measured in some time points. Each thickness value has been obtained by an average of 20 measures, see figure 2 for two measures of them, and we have obtained the following values:

TABLE 2. Patina thickness measures.

Time of measure (hours)	Averaged value (cm)	Standard deviation
8	$5.4418 \cdot 10^{-4}$	$1.7331 \cdot 10^{-4}$
24	$9.2672 \cdot 10^{-4}$	$1.8473 \cdot 10^{-4}$
40	$13.2522 \cdot 10^{-4}$	$2.4102 \cdot 10^{-4}$

Then, we used the least square method to find the best parameters. We obtained (in cm^2/sec): $D_g = 9.9 \cdot 10^{-9}$, $D_s = 3.96 \cdot 10^{-5}$, $D_o = 9.9 \cdot 10^{-6}$ and $D_w = 3.96 \cdot 10^{-5}$. The evolution in time of the corrosion products thickness is in figure 4. We can see the difference between the experimental points

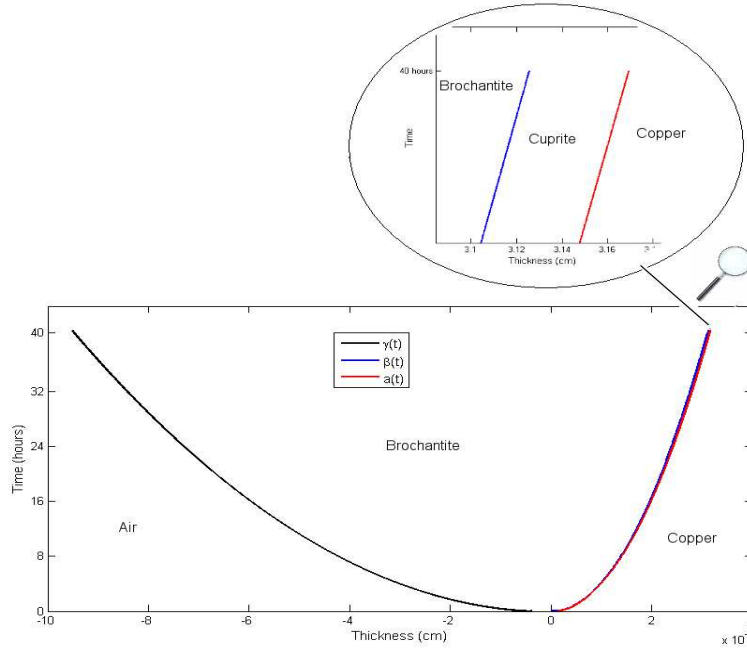


FIGURE 4. Evolution of $\gamma(t)$, $\beta(t)$ and $a(t)$.

and the best simulation in figure 5

Remark Here, we test numerical scheme to reproduce the chemical reactions in eqs. (1) and (3). Simulations, after 40 hours, give us the following values: $\gamma = -9.505 \cdot 10^{-4}$ (cm), $a = 3.1693 \cdot 10^{-4}$ (cm), $b = 7.9916 \cdot 10^{-4}$ (cm). Knowing the molar volume of copper $V_c = \rho_c/M_c$, cuprite $V_p = \rho_p/M_p$, and brochantite $V_b = \rho_b/M_b$, we find that the number of copper moles wasted are $a/V_c = 4.4588 \cdot 10^{-5}$, the number of cuprite moles formed are $b/V_p = 2.2294 \cdot 10^{-5}$, i.e. two copper moles are wasted to form one cuprite mole, as we expect from eq. (1). Similarly, we obtain the number of cuprite moles wasted by reaction (3) is $b/V_p = 2.2173 \cdot 10^{-5}$, while the number of

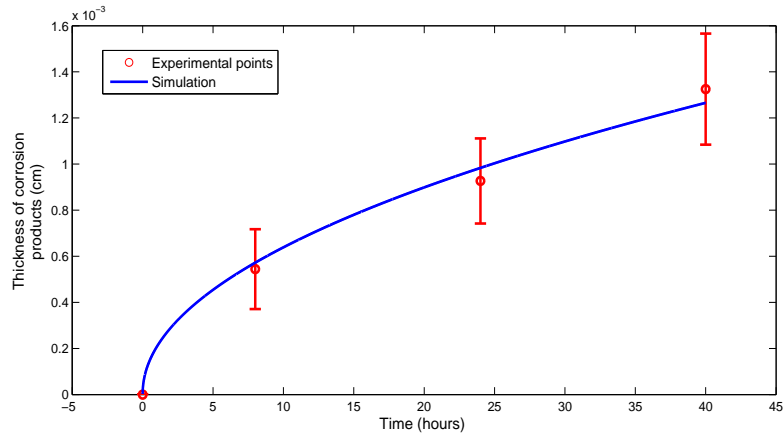


FIGURE 5. Simulation (continuous line) and experimental points (in red).

brochantite moles formed by the same reaction is $h_b/V_b = 1.1086 \cdot 10^{-5}$, i.e. for each brochantite mole formed two cuprite moles are wasted, as expected from (3).

5. APPLICATION

In this section we assume to use the calibrated model with environmental data, detected in Rome at Piazzale Fermi during the year 2005. This application is just an example on how the model can be used. Since the model has been calibrated for high relative humidity and SO_2 concentration, the calibration should be improved by experiments with lower values of relative humidity and SO_2 concentration. The SO_2 concentration detected is in figure 6 and the temperature is in figure 7.

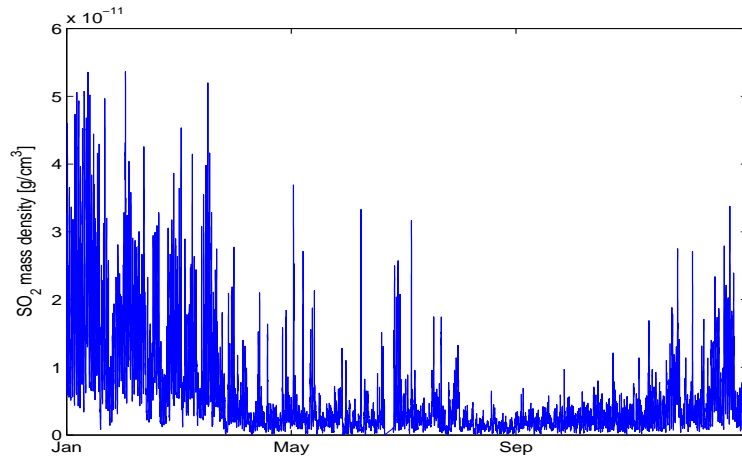


FIGURE 6. SO_2 concentration detected at Piazzale Fermi (Rome, Italy) during the 2005.

Assuming to have a good calibration with our environmental data, we need of saturated vapor density (SVD in $[g/cm^3]$) as function of

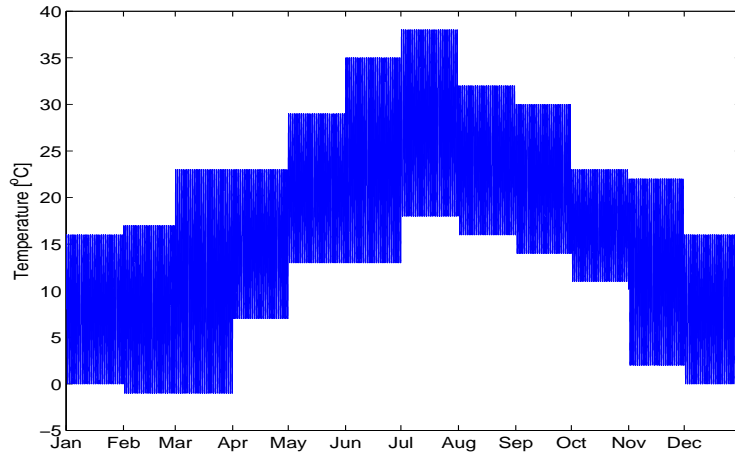


FIGURE 7. Temperature detected at Piazzale Fermi (Rome, Italy) during the 2005.

relative humidity and temperature T [$^{\circ}\text{C}$] detected at Piazzale Fermi. It is useful for getting an exact quantity of water vapor in the air from a relative humidity (RH), the density of water in the air is given by $RH \cdot SVD = \text{ActualVaporDensity}$. The behavior of water vapor density is a non-linear function, but an approximate calculation of saturated vapor density can be made from an empirical fit of the vapor density curve 50 (between $0 - 45$ $^{\circ}\text{C}$ is a good approximation).

$$(50) \quad SVD(T) = 5.018 + 0.32321T + 8.1847 \cdot 10^{-3}T^2 + 3.1243 \cdot 10^{-4}T^3.$$

The figure of saturated vapor density obtained is in figure 8

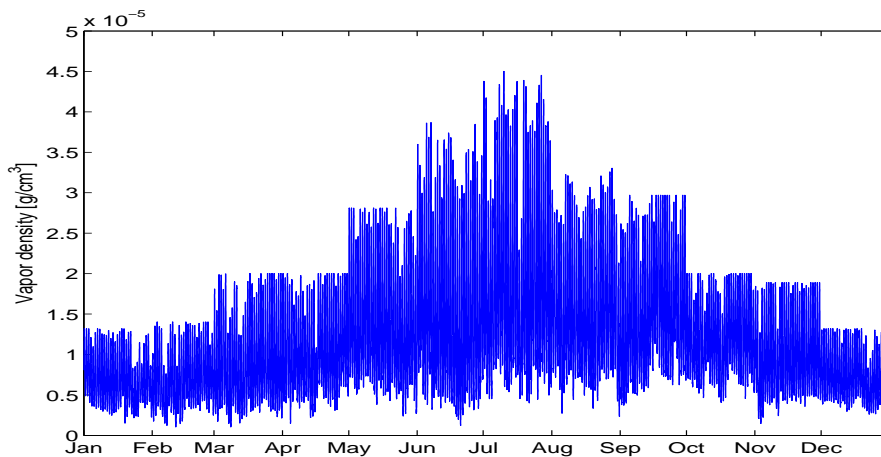


FIGURE 8. Saturated vapor density obtained by temperature and relative humidity detected at Piazzale Fermi (Rome, Italy).

Thus, using SO_2 , temperature and humidity data detected at Piazzale Fermi in Rome during the 2005, we obtained the behavior of corrosion products illustrated in figure 9.

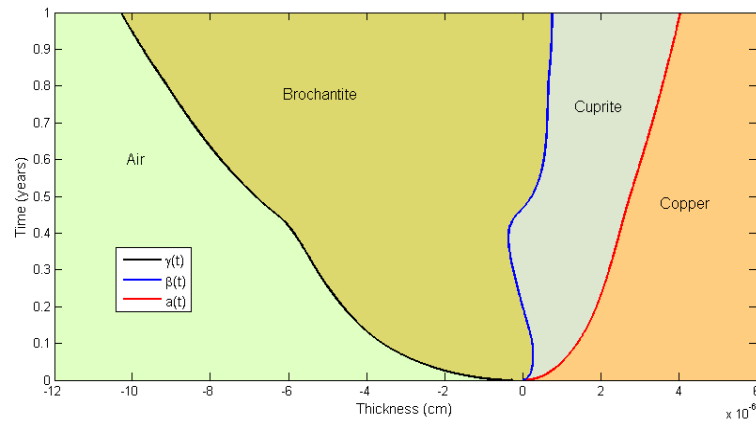


FIGURE 9. Simulation of corrosion with environmental data detected at Piazzale Fermi (Rome, Italy) in 12 months (2005).

Results of this simulation represent a qualitative example of corrosion formation on copper under SO_2 attack. They have to be improved by others laboratory experiments, because our model is calibrated using a very high SO_2 concentration (never present in the atmospheric environment in this concentration), and under a very high relative humidity (near to 100%). To have a more accurate calibration, it would be necessary set up mainly experiments with different SO_2 concentration and different concentration of humidity in the air, so to calibrate the model under these variations.

Our conditions produce a very thick cuprite layer in 1-year simulations with respect to the laboratory experiments, because of the air SO_2 concentration is very lower than that present in the experimental room, and this caused a slower growth of brochantite layer.

6. CONCLUSIONS

In conclusion a new mathematical model was developed to describe and simulate the evolution of brochantite formation on Cultural Heritage artifacts exposed to sulfur dioxide atmosphere. The aim was to create a new approach to forecasting corrosion behavior without the necessity of an extensive use of laboratory testing using chemical-physical technologies, while taking into account the main chemical reactions. Although the model was kept simple, just describing the main reaction and transport processes involved, the mathematical simulations and the related model calibration are in agreement with the laboratory experiments.

REFERENCES

- [1] T. Aastrup, M. Wadsak, C. Leygraf and M. Schreiner; In Situ Studies of the Initial Atmospheric Corrosion of Copper Influence of Humidity, Sulfur Dioxide, Ozone, and Nitrogen Dioxide, *J. Electrochem. Soc.* **147**(7) (2000), pp. 2543-2551;
- [2] M. Briani, R. Natalini and G. Russo; Implicit-explicit numerical schemes for jump-diffusion processes, *Calcolo*, **44** (2007), pp.33-57.
- [3] S.K. Chawla, J.H. Payer; The early stage of atmospheric corrosion of copper by sulfur dioxide, *J. Electrochem. Soc.*, **137**:1 (1990).
- [4] C. Chiavari, A. Colledan, A. Frignani, G. Brunoro; Corrosion evaluation of traditional and new bronzed for artistic casting, *Mater. Chem.Phys.* **95** (2006), 252.
- [5] C. Chiavari, E. Bernardi, C. Martini, F. Passarini, F. Ospitali, L. Robbiola; The atmospheric corrosion of quaternary bronzes: the action of stagnant rain water, *Corrosion Science*, **52**, (2010), pp.3002-3010.
- [6] F. Clarelli, A. Fasano, R. Natalini; Mathematics and Monument Conservation: Free Boundary Models of Marble Sulfation; *SIAM Journal of Applied Mathematics*, **69** (1), (2008), pp. 149-168.
- [7] B. De Filippo, L. Campanella, A. Brotzu, S. Natali, D. Ferro; Characterization of bronze corrosion products on exposition to sulphur dioxide; *Advanced Materials Research*, **138** , (2010), pp. 21-28.
- [8] B. De Filippo, A novel approach for the study of the characterization of the corrosion patina on bronze samples exposed to sulphur dioxide corrosion atmosphere, *Ph.D Thesis*, Università di Rome "La Sapienza", (2011).
- [9] L. A. Farrow, T.E. Graedel and C. Leygraf; Gildes model studies of aqueous chemistry. II. The corrosion of zinc in gaseous exposure chambers, *Corrosion Science*, **38** (12), (1996), 2181.
- [10] K.P. Fitzgerald, J. Nairn, A. Atrens; The chemistry of copper patination, *Corros. Sci.*, **40**, 12, (1998), pp. 2029-2050.
- [11] K.P. Fitzgerald, J. Nairn J., G.A. Skennerton, Atmospheric corrosion of copper and the colour, structure and composition of natural patina on copper, *Corros. Sci.*, **48**, (2006), pp. 2480-2509.
- [12] T.E. Graedel, J.P. Franey, G.W. Kammlott; The corrosion of copper by atmospheric sulphurous gases, *Corros. Sci.*, **23**:11, (1983), 1141.
- [13] T.E. Graedel, J.P. Franey, G.J. Gualtieri, G.W. Kammlott and D.L. Malm; On the mechanism of silver and copper sulfidation by atmospheric H_2S and OCS, *Corros. Sci.*, **25**:12, (1985), 1163.
- [14] T.E. Graedel, K. Nassau, J.P. Franey; Copper Patinas Formed in the Atmosphere-I. Introduction, *Corros. Sci.*, **27**, No. 7, (1987), pp. 639-657.
- [15] T. E. Graedel; Gildes Model studies of Aqueous Chemistry I. Formulation and potential applications of the multi-regime model. *Corrosion Science*, **38**:12, (1996), 2153.
- [16] A. Kratschmer, I. Odnevall Wallander, C. Leygraf; The evolution of outdoor copper patina, *Corros. Sci.*, **44**, (2002), pp. 425-450.
- [17] R.S. Larson; A Physical and Mathematical Model for the Atmospheric Sulfidation of Copper by Hydrogen Sulfide, *J. Electrochem. Soc.* **149** (2), (2002), pp. B40-B46.

- [18] I.D. Mac Load; Bronze Disease: an electrochemical explanation, *ICCM Bulletin*, **7** (1), (1981), p. 16.
- [19] K. Nassau, A.E. Miller, T.E. Graedel; The reaction of simulated rain with copper, copper patina, and some copper compound, *Corros. Sci.*, **27**, (1987), pp. 703-719.
- [20] I. Odnevall and C. Leygraf; Atmospheric Corrosion of Copper in a Rural Atmosphere, *Journal of The Electrochemical Society*, **142**, (1995), pp. 3682-3689.
- [21] J.H. Payer, G. Ball, B.I. Rickett, H.S. Kim; Role of transport properties in corrosion product growth; *Materials Science and Engineering*, **A198**, (1995), p.91.
- [22] J.H. Payer; Corrosion processes in the development of thin tarnish films; *Proceedings of the Thirty Sixth IEEE Holm Conference on Electrical Contacts meeting jointly with the Fifteenth International Conference on Electrical Contacts*, Piscataway, NJ: IEEE, (1990) pp. 203-211.
- [23] S.J. Ruuth; Implicit explicit methods for reaction-diffusion problems in pattern formation, *J. Math. Bio.*, **34**, (1995), pp. 148-176.
- [24] I. Sandberg, I. Odnevall Wallinder, C. Leygraf, N. Le Bozec; Corrosion-induced copper runoff from naturally and pre-patinated copper in a marine environment, *Corros. Sci.*, **48**, (2006), pp. 4316-4338.
- [25] D.A. Scott; Copper and Bronze in art: Corrosion, Colorants, Conservation, *The Getty Conservation Institute*, Los Angeles, ISBN 0-89236-638-9 (2002).
- [26] J. Tidblad and T.E. Graedel; Gildes Model Studies of Aqueous Chemistry. III. Initial So₂-Induced Atmospheric Corrosion of Copper, *Corros. Sci.* **38**:12, (1996), p. 2201.
- [27] M. Watanabe, M. Tomita, and T. Ichino; Characterization of Corrosion Products Formed on Copper in Urban, Rural/Coastal, and Hot Spring Areas *Journal of The Electrochemical Society*, **148** (12), (2001), pp. B522-B528.
- [28] M. Watanabe, Y. Higashi, and T. Ichino; Surface Observation and Depth Profiling Analysis Studies of Corrosion Products on Copper Exposed Outdoors, *Journal of The Electrochemical Society*, **150**, (2003), pp. B37-B44 .

ISTITUTO PER LE APPLICAZIONI DEL CALCOLO "M. PICONE", CONSIGLIO NAZIONALE DELLE RICERCHE POLO SCIENTIFICO - EDIFICIO F CNR VIA MADONNA DEL PIANO 10; I-50019 SESTO FIORENTINO (FI), ITALY.

ISTITUTO PER LE APPLICAZIONI DEL CALCOLO "M. PICONE", CONSIGLIO NAZIONALE DELLE RICERCHE, VIA DEI TAURINI 19, I-00185, ROMA, ITALY.

ISTITUTO PER LE APPLICAZIONI DEL CALCOLO "M. PICONE", CONSIGLIO NAZIONALE DELLE RICERCHE, VIA DEI TAURINI 19, I-00185, ROMA, ITALY.